Grain Nucleation and Growth During Phase Transformations

S. E. Offerman,[1,2]* N. H. van Dijk,[1] J. Sietsma,[2] S. Grigull,[3] E. M. Lauridsen,[4] L. Margulies,[3,4] H. F. Poulsen,[4] M. Th. Rekveldt,[1] S. van der Zwaag[2]

The mechanical properties of polycrystalline materials are largely determined by the kinetics of the phase transformations during the production process. Progress in x-ray diffraction instrumentation at synchrotron sources has created an opportunity to study the transformation kinetics at the level of individual grains. Our measurements show that the activation energy for grain nucleation is at least two orders of magnitude smaller than that predicted by thermodynamic models. The observed growth curves of the newly formed grains confirm the parabolic growth model but also show three fundamentally different types of growth. Insight into the grain nucleation and growth mechanisms during phase transformations contributes to the development of materials with optimal mechanical properties.

Grain nucleation and growth are important phenomena in polycrystalline materials such as metals and most ceramics. They govern the kinetics of many phase transformations and recrystallization processes that take place during processing. The final average grain size after the transformation is directly related to the strength of the material. In general, a smaller average grain size results in a stronger material. Despite the various transformation models that have been proposed in the past 60 years, the kinetics of these phase transformations is still poorly understood. Most of these models are based on the classical nucleation theory (CNT) (*1*) and the law of parabolic grain growth as derived by Zener (*2*), which describe the behavior of individual grains in the bulk of the material.

The experimental techniques that have been available to verify these nucleation and growth models are limited to either observations at the surface or the determination of the average grain growth behavior in the bulk (*3*). The development of x-ray microscopes at synchrotron sources with focused high-energy x-rays has created the opportunity to study individual grains in the bulk of a material (*4*–*7*). In addition, these measurements give unique information about the grain nucleation during the phase transformation. Because of a combination of fundamental scientific interest and technological importance, the phase transformations in steel have been investigated more extensively than those in any other material, and steel is the material studied here.

Carbon steel consists of iron and carbon [up to 2 weight % (wt %)], with small quantities of alloying elements, and exists in three stable crystalline phases: austenite with a face-centered cubic structure, ferrite with a body-centered cubic structure, and cementite (Fe_3C) with an orthorhombic structure. The principal transformation reaction in steel, which is a typical diffusion-controlled solid-state transformation, is from the high-temperature austenite phase to the low-temperature ferrite phase. Because the solubility of carbon in ferrite is much lower than in austenite, the transformation is accompanied by a carbon enrichment of the austenite. At lower temperatures, the carbon-rich austenite decomposes into pearlite, which consists of a lamellar structure of two interpenetrating single crystals of ferrite and cementite (Fig. 1).

In order to study the time evolution of individual grains during the phase transformations, a relatively small volume of steel was illuminated with a monochromatic beam of hard x-rays from a synchrotron source. Through a slight rotation of the sample around an axis perpendicular to the beam, a number of grains gave rise to diffraction spots on a two-dimensional detector. Figure 2 shows a diffraction pattern halfway through the austenite-to-ferrite transformation. From the standard diffraction theory it can be shown that the intensity of each spot is proportional to the volume of the grain it originates from. The intensity of the spot is normalized with respect to the total intensity of the diffraction ring at the end of the transformation (*4*), by assuming that the equilibrium ferrite fraction is then reached. By repeated acquisition of images, the nucleation and growth of the individual grains were studied, with a typical time resolution of 10 s.

The steel was annealed at 900°C for 10 min in order to form the austenite phase and was subsequently continuously cooled to 600°C in 1 hour. By counting the number of valid diffraction spots, the number of ferrite grains (with a grain radius above the detection limit of about 2 μm) was obtained as a function of temperature (Fig. 3A). The number of ferrite nuclei increased most rapidly just below the austenite/ferrite transition temperature of 822°C for this steel, but new ferrite nuclei were continuously formed over a large temperature range until the austenite/pearlite transformation started at 685°C. Only a very small number of new pearlitic ferrite nuclei were formed in the pearlite transition temperature range. Figure 3B shows the normalized experimental nucleation rate, which is compared to the CNT (*1*). The shape of the theoretical curve is in qualitative agreement with the measurements. The most striking

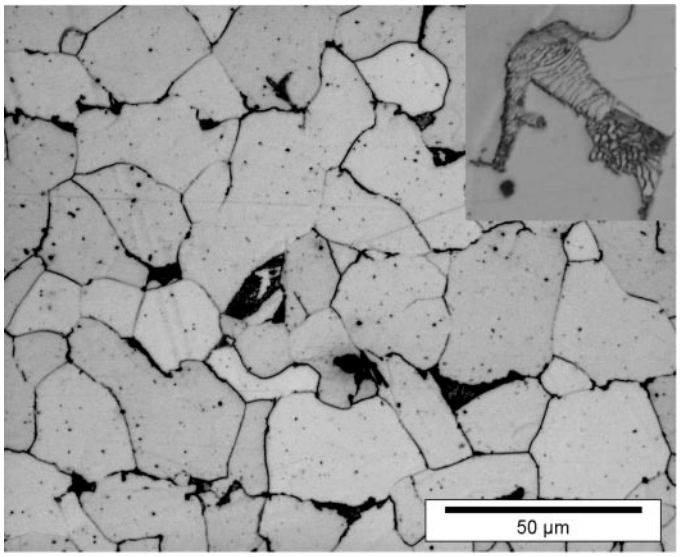

Fig. 1. Optical microscopy images of the construction steel (0.21 wt % C, 0.51 wt % Mn, and 0.20 wt % Si) at room temperature. The light regions correspond to ferrite and the dark regions to pearlite. The insert in the top right corner shows the lamellar structure of pearlite (magnification is three times that of the main image).

[1]Interfaculty Reactor Institute, Delft University of Technology, Mekelweg 15, 2629 JB Delft, Netherlands. [2]Department of Materials Science, Delft University of Technology, Rotterdamseweg 137, 2628 AL Delft, Netherlands. [3]European Synchrotron Radiation Facility, BP 220, 38043 Grenoble Cedex, France. [4]Center for Fundamental Research: Metal Structures in 4D, Materials Research Department, Risø National Laboratory, 4000 Roskilde, Denmark.

*To whom correspondence should be addressed. E-mail: Offerman@IRI.TUDelft.nl

difference is that the maximum nucleation rate occurred at a higher temperature than predicted by the CNT.

According to the CNT, the driving force for nucleation is the decrease in Gibbs free energy per unit of volume of the system during the phase transformation Δg_V, which depends on the chemical composition and temperature. However, the creation of a new nucleus also requires energy because of the formation of an interface between the nucleus and the original phase. According to the CNT, the nucleation rate can be expressed as

$$\frac{dN}{dt} \propto (1-f)\,\frac{kT}{h}\exp\left[-\frac{\Delta G^* + Q_D}{kT}\right] \quad (1)$$

where the factor $(1-f)$ takes into account the decrease in the number of potential nucleation sites with increasing fraction f (in this case, the ferrite fraction f^α), k is the Boltzmann constant, h is the Planck constant, and T is the temperature. The mobility of the (iron) atoms in the original (austenite) phase is taken into account by the activation energy for diffusion Q_D. The energy that is necessary to form a critical nucleus is referred to as the activation energy for nucleation ΔG^*, which can in general be written as $\Delta G^* = \Psi/\Delta g_V^2$. The factor Ψ accounts for the energy of the interface (boundary) between the nucleus and the original phase and the geometry of the nucleus.

It is the uncertainty in Ψ that makes predictions of the nucleation rate very difficult, so models have been developed in order to estimate Ψ (*8*, *9*). These models have in common that a certain shape is assumed for the nucleus, which is then applied to all the nuclei in the system. One of the early models by Clemm and Fisher (*8*) predicts $\Psi_{CF} = 3.3 \times 10^{-3}$ J^3/m^6 for grain corner nucleation of nuclei with incoherent grain boundaries. A more recent model by Lange *et al.* (*9*) gives $\Psi_{LEA} = 2.1 \times 10^{-6}$ J^3/m^6 for a pillbox shape of the nucleus with coherent and semicoherent interfaces. A best fit of our experimental data to Eq. 1 gives $\Psi_{exp} = 5 \times 10^{-8}$ J^3/m^6, when $Q_D = 4.72 \times 10^{-19}$ J (*10*). This means that the activation energy for nucleation as determined in this experiment is at least two orders of magnitude smaller than the models predict.

The difference between experiment and theory cannot solely be explained by varying Δg_V and/or Q_D within a realistic range. The low experimental value for the activation energy for nucleation indicates a close balance between the energy that is released by the removal of incoherent austenite/austenite grain boundaries and the energy that is required for the formation of coherent and incoherent austenite/ferrite grain boundaries. This could be related to recent computer simulations of nucleation in a system of colloidal particles. These calculations indicate that it is possible that the initial nucleus has a metastable crystallographic structure, which transforms in a stable structure upon growth (*11*). Moreover, it may be questioned whether conventional continuum thermodynamics accurately predicts the driving force Δg_V, because the critical nucleus only consists of 10 to 100 atoms.

We determined the growth behavior of individual ferrite grains and pearlite colonies by continuously monitoring the intensity of the diffraction spots (Fig. 4). The ferrite grain volume V^α that was derived from the measured intensity is transformed into a grain radius R^α by assuming that the grain shape is spherical. Four types of ferrite growth could be distinguished, as shown in the four panels of Fig. 4. In each panel, the experimental growth curves are compared with the theoretical prediction of the classical Zener model (*2*), which predicts a parabolic growth for a spherical grain when the growth rate is limited by diffusion. This theory is commonly used to describe the growth of ferrite grains in construction steels during the transformation from austenite. Because the solubility of carbon in ferrite is two orders of magnitude lower than in austenite, the carbon

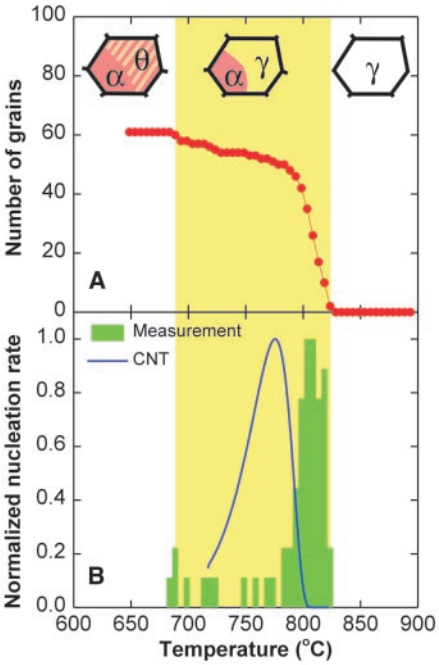

Fig. 3. Nucleation as a function of temperature during continuous cooling of the steel from 900° to 600°C in 1 hour. (**A**) The total number of valid ferrite reflections. (**B**) The normalized experimental nucleation rate (green bars) compared to the CNT (line) as given by Eq. 1. The ferrite fraction f^α was assumed to develop according to thermodynamic equilibrium and was calculated from the thermodynamic database MTDATA. The driving force for nucleation Δg_v was determined through the parallel-tangent construction with the standardized data from the Scientific Group Thermodata Europe (SGTE) under the assumption that the alloying elements were homogeneously distributed. For Ψ, the value determined by Lange *et al*. (*9*) was used: $\Psi_{LEA} = 2.1 \times 10^{-6}$ J^3/m^6. The nucleation rate was normalized to the maximum nucleation rate. The first ferrite reflections were observed at a temperature of 822°C and the pearlite started to form at 685°C. The different stages during the phase transformations in steel are schematically drawn at the top of the figure, which shows the three phases: austenite (γ), ferrite (α), and cementite (θ).

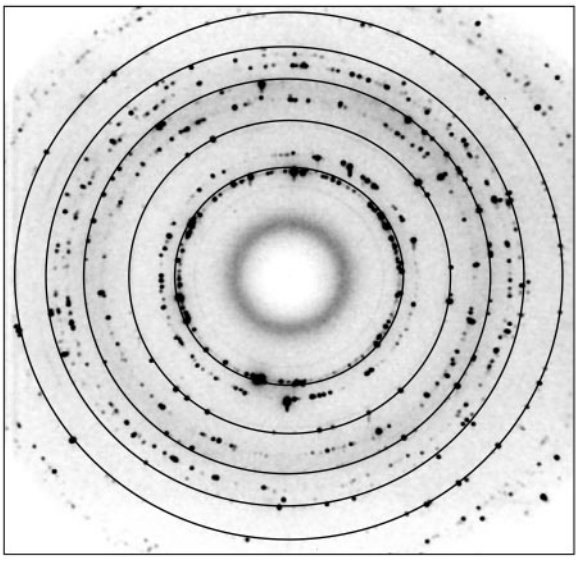

Fig. 2. X-ray diffraction pattern of the steel showing the austenite and ferrite reflections at 763°C. The solid rings indicate the expected scattering angles from the ferrite grains illuminated by the x-ray beam. The energy of the monochromatic x-rays corresponded to 80 keV (with a wavelength of 1.55×10^{-2} nm), the beam size to 94×97 μm^2, and the thickness of the sample to 400 μm. During the exposure, the sample was continuously rotated around the vertical axis over an angle from –0.8° to 0.8°. In order to determine whether a diffraction spot was valid, we took additional exposures for rotation angles from –2.4° to –0.8° and 0.8° to 2.4°, which told us whether the complete integrated intensity was observed in the central exposure. Once every six exposures, the beam size was expanded to 139×139 μm^2 in order to check whether the total volume of the grain was illuminated by the small central beam. For the experiment, we used the three-dimensional x-ray diffraction microscope (3DXRD) at beam line ID11 of the European Synchrotron Radiation Facility in transmission geometry.

piles up at the moving interface and diffuses into the bulk of the austenite phase. This forms the rate-limiting process for the ferrite grain growth during the phase transformation. According to the Zener model, R^{α} as a function of time t is given by

$$R^{\alpha}(t) = \chi \sqrt{D_C^{\gamma}(t - t_s)} \qquad (2)$$

where, in the case of the austenite/ferrite transformation, χ is a parameter that is determined by the carbon solubilities in ferrite and austenite; D_C^{γ} is the carbon diffusion coefficient in the bulk of the austenite, which depends on temperature and carbon concentration (*12*); and t_s is the moment of nucleation of the grain. Equation 2 only applies to the initial stages of the transformation, during which the growth of the individual grain is not limited by interactions with neighboring grains because of overlapping diffusion fields (soft impingement) or existing grain boundaries (hard impingement).

The first and most frequently observed type of ferrite grain growth is initially in agreement with the theory (Fig. 4A). This means that the grains initially do not interact with growing neighboring grains. For each of the grains, the growth curves start to deviate from the Zener theory at different levels, depending on the local impingement conditions. Figure 4B shows the second type of growth, in which some ferrite grains continue to grow with the same crystallographic orientation during the pearlite formation as part of a pearlite colony. This remarkable behavior has so far only been observed by Thompson and Howell (*13*), who performed transmission electron microscopy measurements at the interface between ferrite and pearlite. This mechanism of continued growth of preexisting ferrite appears to be the dominant mechanism for pearlite formation. This is evidenced by the fact that very few new pearlite nuclei were found in the pearlite transformation temperature range (Fig. 3A). These growth curves also show that the pearlite colony reaches a larger final size when the initially formed ferrite grain is smaller. Another difference between the austenite/ferrite and austenite/pearlite transformation is that at the low imposed cooling rate, all the pearlite colonies start to grow at a well-defined temperature of 685°C for this steel. Once pearlite formation is initiated, the intercalated cementite takes up all the carbon, which increases the growth rate.

The final two types of grain growth have not been observed or postulated before. Figure 4C shows the third type of ferrite growth, in which ferrite nucleation and growth are retarded. An enrichment of carbon in the austenite causes a local decrease in transition temperature, which leads to retarded nucleation. The retarded growth is caused by indirect interaction with growing neighboring grains. The neighboring grains do not directly touch each other but interfere via surrounding diffusion and stress fields (*14*). The last class of ferrite grain growth is characterized by complex growth behavior (Fig. 4D). In this least frequently observed growth mode, ferrite grains not only grow but also temporarily shrink upon continued transformation. This behavior is due to a complex grain-boundary migration caused by direct interaction with neighboring grains. The neighboring grains directly touch, but their grain boundaries are not yet in their equilibrium position. It is known that some grain boundaries are more stable than others, depending on the curvature (*15*). Because the growth is a dynamic process, the forces on the grain boundaries may change irregularly, resulting in the growth behavior shown in Fig. 4D. Thus, on the level of individual grains we can distinguish four types of grain growth: There are grains that do not interact with neighboring grains, grains that continue to grow with the same crystallographic orientation into another phase, grains that indirectly interact, and grains that directly interact with neighboring grains.

Our measurements show that the activation energy for grain nucleation is at least two orders of magnitude smaller than that predicted by thermodynamic models. The observed growth curves of the newly formed grains confirm the parabolic growth model but also show three fundamentally different types of growth. We conclude that the current models do not accurately predict the phase transformation kinetics in polycrystalline materials. Future nucleation models should give a better prediction of the optimum size and shape of the critical nucleus, which initially may have a metastable crystallographic structure, with respect to the energy of the interfaces. Future growth models should incorporate the interactions between growing neighboring grains. From a technological perspective, these new insights are of importance to the modern materials production process, which relies heavily on grain nucleation and growth models to produce tailor-made materials.

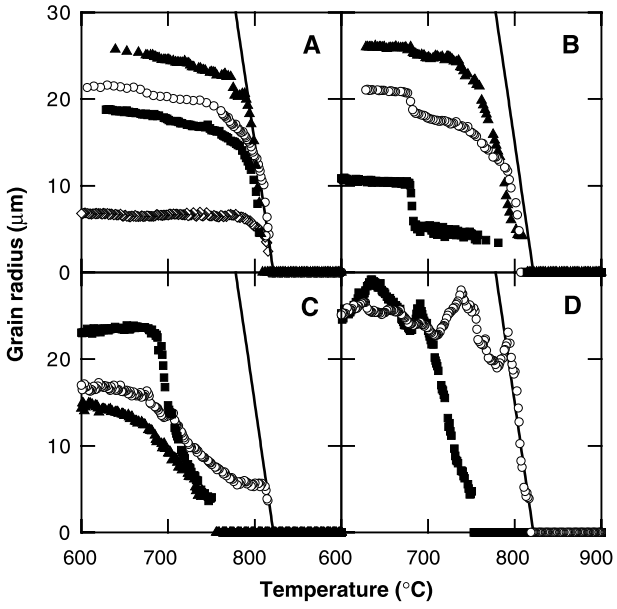

Fig. 4. Particle radius of individual ferrite grains as a function of temperature during continuous cooling of the steel from 900° to 600°C in 1 hour. Symbols indicate the growth curves of individual grains, and the solid line indicates the Zener theory. (**A**) Ferrite grains that started to grow according to the classical Zener theory (line). (**B**) Ferrite grains that continued to grow with the same crystallographic orientation during the pearlite formation as part of a pearlite colony. (**C**) Retarded ferrite growth. (**D**) Complex ferrite growth.

References and Notes

1. J. W. Christian, *The Theory of Transformations in Metals and Alloys* (Pergamon, Oxford, 1981).
2. C. Zener, *J. Appl. Phys.* **20**, 950 (1949).
3. C. E. Krill III *et al.*, *Phys. Rev. Lett.* **86**, 842 (2001).
4. E. M. Lauridsen, D. J. Jensen, H. F. Poulsen, U. Lienert, *Scripta Mater.* **43**, 561 (2000).
5. L. Margulies, G. Winther, H. F. Poulsen, *Science* **292**, 2392 (2001).
6. H. F. Poulsen *et al.*, *J. Appl. Crystallogr.* **34**, 751 (2001).
7. B. C. Larson, W. Yang, G. E. Ice, J. D. Budal, J. Z. Tischler, *Nature* **415**, 887 (2002).
8. P. C. Clemm, J. C. Fisher, *Acta Metall.* **3**, 70 (1955).
9. W. F. Lange III, M. Enomoto, H. I. Aaronson, *Metall. Trans. A* **19A**, 427 (1988).
10. J. Kučera, K. Stránský, *Mater. Sci. Eng.* **52**, 1 (1982).
11. S. Auer, D. Frenkel, *Nature* **409**, 1020 (2001).
12. J. Ågren, *Scripta Metall.* **20**, 1507 (1986).
13. S. W. Thompson, P. R. Howell, *Scripta Metall.* **22**, 1775 (1988).
14. M. Onink, F. D. Tichelaar, C. M. Brakman, E. J. Mittemeijer, S. van der Zwaag, *J. Mater. Sci.* **30**, 6223 (1995).
15. D. A. Porter, K. E. Easterling, *Phase Transformations in Metals and Alloys* (Chapman and Hall, London, 1981).

16. We thank S. O. Kruijver and L. Zhao for assistance during the synchrotron measurements, S. Schmidt for the use of his software, and E. R. Peekstok for the optical microscope images. Financially supported in part by the Foundation for Technical Sciences (STW) of the Netherlands Organisation for Scientific Research (NWO), the Danish National Research Foundation, and the Danish Research Council SNF (via Dansync).

29 July 2002; accepted 20 September 2002